Triangular-patch model of bowtie antennas: validation against Brown and Woodward

C.J.Leat
N.V.Shuley
G.F.Stickley

Indexing terms: Bowtie antennas, Validation, Biconical antennas

Abstract: Input impedance and field patterns for bowtie antennas of various lengths and flare angles have been calculated using the moment method and triangular basis functions. These results agree to within 10% of previous experimental results. Rao–Wilton–Glisson basis functions, delta-gap feed and Caorsi's line-integral method were used.

1 Introduction

The bowtie antenna is a commonly used broadband radiating element. Research on its application and modelling almost invariably cites the 1952 experimental paper by Brown and Woodward [1]. In that paper, experimentally measured driving-point impedances and field patterns were presented for biconical and bowtie antennas for the full range of flare angles, and for electrical monopole lengths ranging from 20 to 270°.

The authors are in the course of developing a moment-method code tailor made for the modelling of antennas on a halfspace. The free-space version presented here is an intermediate stage intended to demonstrate the acceptability of computation-saving methods to be carried into the halfspace code. Although the scarcity of benchmark data on commercial software makes it difficult to compare speed and accuracy, it is the authors' belief that the code presented is at least as fast as commercial codes. The use of point matching, a line-integral method for the self terms [2] and delta-function sources for the interaction between well separated patches is shown to give acceptable results in the comparison with [1]. Furthermore, in making the comparison, some of the methods used in [1] are considered critically and shown to be erroneous.

2 Moment-method model

The method used was essentially that given in [3], so only those aspects not covered in the reference will be given here. A triangular basis-function diagram based on [3] is included as Fig. 1.

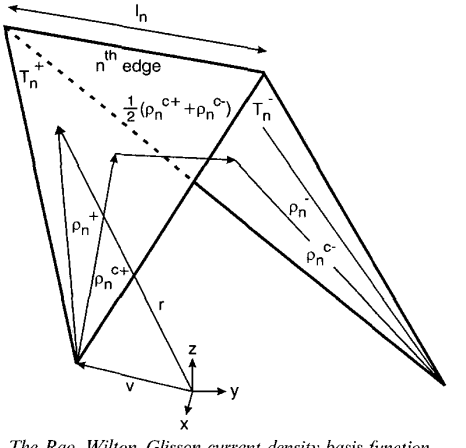

Fig. 1 *The Rao–Wilton–Glisson current-density basis function*
The diagram shows a triangle pair forming a bent surface sharing an internal edge. The sheet-current density at any point T_n^+ is $(l_n/(2A_n^+))\ \rho_n^+$ assuming unit magnitude of the basis function. The associated charge density is uniform and equal to $l_n/(A_n^+ i\omega)$

One detail not covered in [3] was the method of integrating the Green's-function singularity when the field point is in the source triangle, as happens in the calculation of the self terms. Several papers have been published dealing with the problem. Wilton *et al.* [4] removed the singular (static) part of the scalar and vector potential integrals and converted them to a line integral, the remainder being integrated numerically over the triangle. Graglia [5] extended this approach to include the gradients of the Green's functions as kernels, thus extending the approach to include its application to electric-field integral-equation (EFIE) methods. For a fully Galerkin approach, Eibert and Hansen [6] supply analytical formulas for the double integration of the static Green's function.

The method developed in Caorsi *et al.* [2] was used in the present work. It converts the whole dynamic Green's function area integral to a line integral.

The Caorsi *et al.* method converts both self- and off-diagonal Green's function and gradient integrals into line integrals, but is particularly simple when applied to the self terms, when only electric sources are present and when the mixed-potential method is used. The simplified geometry obtained when the self term is considered is shown in Fig. 2. Note that the distance h in [2] is zero in the self-term case, and is not included in Fig. 2.

IEE Proceedings online no. 19981881

Paper first received 9th September 1997 and in revised form 13th Janaury 1998

The authors are with the Department of Computer Science and Electrical Engineering, University of Queensland, 4072, Australia

C.J. Leat and G.F. Stickley are also with the Centre for Sensor Signal and Information Processing, University of Queensland, Australia

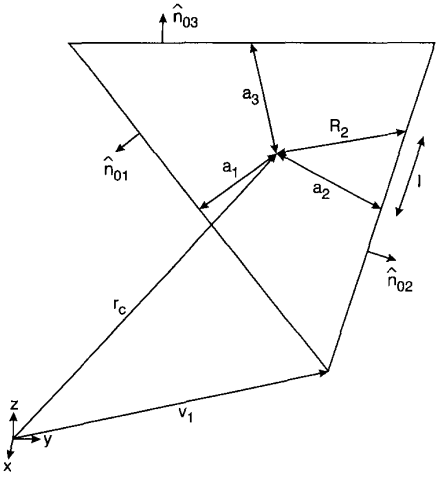

Fig. 2 *Simplified version of the Fig. 3 in [2] for use with self-term integrals*
The field point is at $\mathbf{r}_c$. The integral is computed along the edges in terms of the variable l and makes use of the parameters a_j and normal vectors lying in the plane of the triangle, $\hat{\mathbf{n}}_{0j}$.

The time convention used here is $e^{-i\omega t}$. Dummy variables j, l are used to index local edges and vertices, and so range from 1 to 3. Rao *et al.* [3] used p, q to index field and source triangles and m, n to index edges in the global numbering scheme, and that has been followed here. Note that the area of the same triangle might be referred to as A^q in the triangle-based numbering used during source integration, but as A_n^+ in the edge-based numbering used for current basis functions.

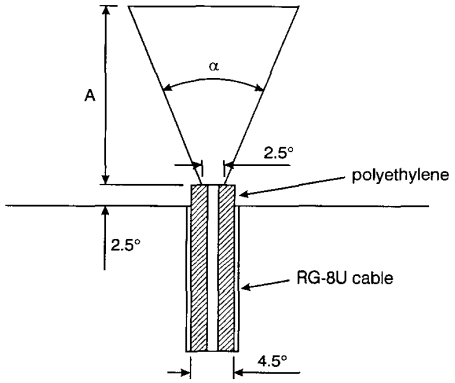

Fig. 3 *Not-to-scale diagram of the feed region used by Brown and Woodward for their monopulse-bowtie impedance measurements*
The electrical dimensions pertain to the measuring frequency of 500 MHz. If the bowtie were a dipole, the feed area would be encased in a cylinder of polyethylene 5° long and 4.5° in diameter. The polarisation in the volume can be thought of as creating a shunt capacitance at the feed.

Suppose that it is desired to calculate the self-term scalar and vector potentials,

$$\Phi_j^{qq} = \frac{l_j}{4\pi i\omega\varepsilon A^q} I^{qq} \tag{1}$$

$$\mathbf{A}_j^{qq} = \frac{\mu l_j}{8\pi A^q} \mathbf{I}_j^{qq} \tag{2}$$

where,

$$I^{qq} = \iint_T \frac{\exp(ik|\mathbf{r}-\mathbf{r}_c|)}{|\mathbf{r}-\mathbf{r}_c|} dS \tag{3}$$

and,

$$\mathbf{I}_j^{qq} = \iint_T (\mathbf{r}-\mathbf{v}_j) \frac{\exp(ik|\mathbf{r}-\mathbf{r}_c|)}{|\mathbf{r}-\mathbf{r}_c|} dS \tag{4}$$

remembering that $\mathbf{r} - \mathbf{v}_j = \boldsymbol{\rho}_j^+$, the vector which forms the basis functions given in [3]. Point matching was used; hence $\mathbf{r}_c$, the centroid of the triangle, is the only field point needed. Readers will recognise eqn. 3 as eqn. 3 in [2] and thus, using eqns. 5 and 10 in [2], and the fact that $h = 0$ and $p = s'$, one obtains

$$I^{qq} = \sum_{j=1}^{3} \int_{\partial_j T} \sum_{m=0}^{\infty} \frac{(ik)^m}{(m+1)!} R_j^{m-1} dl \tag{5}$$

where

$$R_j^2 = a_j^2 + l^2 \tag{6}$$

and $\partial_j T$ is the line which forms the jth edge of the triangle.

Once the scalar integral is computed, eqn. 15 in [3] can be used to calculate the vector-integral term:

$$\mathbf{I}_j^{qq} = \frac{-i}{k} \sum_{l=1}^{3} \hat{\mathbf{n}}_{0l} \int_{\partial_j T} \exp(ikR_l) dl + (\mathbf{r}_c - \mathbf{v}_j) I^{qq} \tag{7}$$

The feed model used was a delta function along one edge which could be described as

$$\mathbf{E} = \hat{\mathbf{y}}\delta(y) \tag{8}$$

where the y axis is a local axis normal to the internal edge along which the field is assumed to exist. A simple feed model where only one edge needs to be driven was used, as shown in Fig. 4.

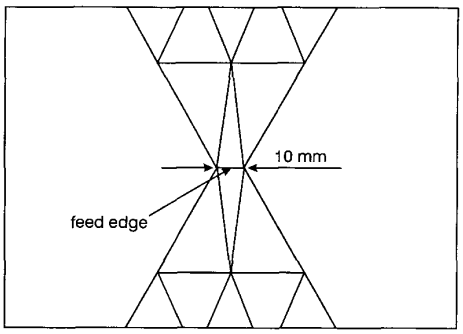

Fig. 4 *Feed region in the dipole-bowtie model*

Kipp and Chan [7] refer to the use of centroid (deltafunction) approximations for the sources when the triangles are sufficiently well separated, thus removing source integration when filling the moment matrix. This can be done if source-to-field distances vary by less than say 20% with very little effect on the computed current distribution. However, in the present work this was also used for all but the self terms with very little difference in the computed current distributions and, for some bowties, convergence appeared to be more rapid.

The idea of using centroid approximations for the sources can also be applied to computation of the fields, once the matrix equation is solved. It is convenient to sum over the basis functions rather than the triangles, however. To compute the far-field radiation patterns, the conducting surface was treated as a set of short dipoles of constant current stretching between the centroids of the triangles adjacent to each edge. The dipole corresponds to the vector $\frac{1}{2}(\boldsymbol{\rho}_n^{c+} + \boldsymbol{\rho}_n^{c-})$. The magnitude of the current is the product of the sheet-current density in the current vector calculated from the moment equation $V = ZI$ and the length of the

edge. For such a short dipole of constant current along its length, the far field is the same as that of an infinitesimal dipole:

$$E_\theta \approx -i\eta k I_n l_n \left| \frac{1}{2}\left(\boldsymbol{\rho}_n^{c+} + \boldsymbol{\rho}_n^{c-}\right) \right| \frac{\exp(ikr)}{4\pi r} \sin\theta \quad (9)$$

where, of course, θ and r refer to the location of the field point in terms of the local spherical co-ordinates relative to the centre of the dipole and the axis $\frac{1}{2}(\boldsymbol{\rho}_n^{c+} + \boldsymbol{\rho}_n^{c-})$. After transformation to the global co-ordinate system, the fields were summed over the complete set of basis functions to produce the plots compared with Brown and Woodward in Figs. 7 and 8.

3 Results and discussion

A number of points need to be stressed regarding the Brown and Woodward paper and the presentation of results. Impedance measurements were made using a monopole over a ground plane at a single frequency (500MHz) using a slotted transmission line to measure the SWR. Today, such experiments would be performed using a VNA sweeping over frequency. The frequency variable in the plots was thus marked as the electrical length of the monopole (dimension A in Fig. 3), and this convention has also been followed here. A result of measuring at a single frequency and physically changing the length of the antenna, as Brown and Woodward did, is that the feed point has a constant electrical dimension.

In the present numerical model, frequency was swept in preference to scaling the mesh. Thus the electrical size of the feed point changed slightly. An enlarged view of the feed area of the mesh is shown in Fig. 4. The feed-point width used was 10mm in a dipole mesh of total length 1m. This corresponds to an electrical length of 2.5° for a monopole length of 125°, which is in the middle of the range of measurement. Regular meshes constructed from 160 isosceles triangles were used for each of the flare angles. The time to fill the matrix, solve the equations and compute field patterns was $\simeq$ 0.5s per frequency point on an Alphastation 4/233 using the centroid approximations for non-self terms. Fully integrated source-current versions consumed about 30 times more CPU time. Much denser triangulations, including Delaunay triangulations with very high density near the edges where currents are concentrated, were also tried, and the results were very similar to those presented here. For dense triangulations, the time consumption increased towards the cube of the number of triangles, $T(s) \approx 1.5 \times 10^{-7} n^3$ being a reasonable estimate.

The raw impedance data from the numerically modelled bowties displayed higher-frequency resonance points than those reported in [1]. This may result from the absence of the projecting coaxial insulation in the model (Fig. 3). However, there are at least two effects influencing the apparent feed point impedance and their combined effect is probably best determined experimentally. (Note that the termination capacitance for this geometry is negative and was estimated to be –0.12pF using the approximation $C_T \approx -0.35 b C_0$ where b is the outer coaxial radius and C_0 is the infinite line capacitance per metre; see section II.10 of [8]. Thus the effect of the projecting dielectric is slightly cancelled). King (section II.9 of [8]) has considered in depth the similar situation of a dipole driven by a two-wire line, with a supporting dielectric stub, and expressed a similar view: King states, 'The theoretical or experimental determination of the actual added capacitance due to a dielectric support and not merely the apparent added capacitance is sufficiently complex to make the accurate evaluation of the contribution to the load by the dielectric support difficult. In practice, to be sure, it is usually only the apparent combined impedance terminating the line that is of interest, and this is readily measured directly in each case.' A constant capacitive reactance was thus added in parallel with the feed. This is appropriate since the constant physical size of the experimental feed area at constant frequency would also have constant capacitive reactance. Brown and Woodward referred to the bowtie reactances being independent of flare angle for a monopole length of 140°. The capacitive reactance required to make the corresponding point on the model data move down to 140° was found to correspond to 0.31pF at 500MHz.

The data in [1] were digitised manually from the published plots using a millimetre rule, and the plots interpolated using a cubic spline.

Figs. 5 and 6 compare half the impedance of the bowtie dipole modelled here with the measurements in [1] for the monopole. Only the curves for flare angles of 10, 30, 50, 70 and 90° are compared, as the figures are too dense if all the plots in [1] are included.

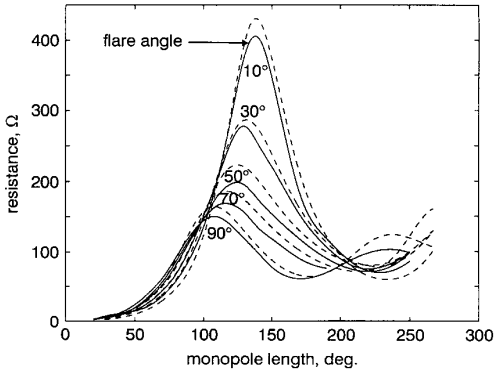

Fig. 5 *Comparison of bowtie-feed-point impedances: resistance*
Brown and Woodward's data for the monopole over ground plane
moment-model plots

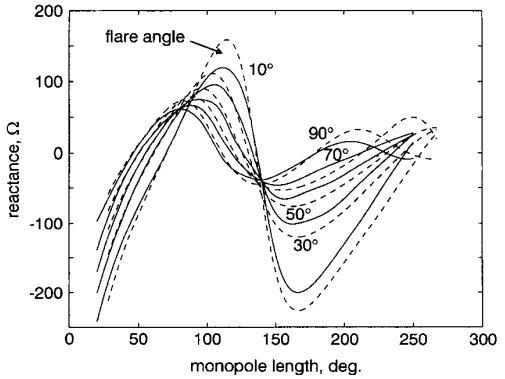

Fig. 6 *Comparison of bowtie-feed-point impedances: reactance*
Brown and Woodward's data for the monopole over ground plane
moment-model plots

The plots can be seen to agree to within 10%. The model data appear to have consistently slightly higher Q-factors than the measured data, displaying a larger one-wavelength resonance resistance and larger

reactance fluctuations. This may result from small losses in the experimental system and imperfect correspondence between the monopole and dipole feed field patterns. Losses due to the finite conductivity of the sheet material ([1] used copper-plated steel sheet) may be included in the calculation of the self-term impedance. ($Z(n, n)$ is increased by the amount

$$\frac{l_n^2 Z_s}{2}\left\{\frac{|\rho_n^{c-}|^2}{A_n^-}+\frac{|\rho_n^{c+}|^2}{A_n^+}\right\}$$

where Z_s is the surface impedance of the material.) However at 500MHz, the sheet resistance of copper is only 5.8mΩ and exerts negligible effect on the impedance; indeed to make a 10% change about 1000 times this value is required. It is possible that losses in the slotted-line measuring apparatus were inadequately calibrated out or that the radiation was more effectively coupled from the frill field of the coaxial feed, than from the delta gap used in the model.

Figs. 7 and 8 compare the field pattern of the 60° flare bowties measured by Brown and Woodward with the calculated pattern from the moment-method model. Two sets of E-plane measurements were published in [1]. One was the variation of electric-field strength as a

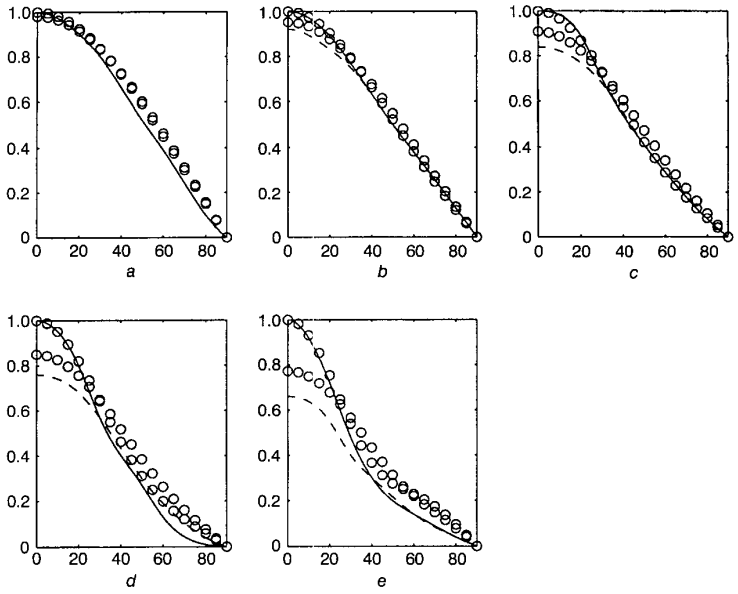

Fig. 7 *Comparison of 60°-flare-angle bowtie field patterns*
The titles refer to the monopole length in electrical degrees
——— Brown and Woodward data for relative electric field strength for plane parallel to bowtie
– – – – Brown and Woodward data for plane normal to bowtie
o moment-model plots
a 60°, *b* 90°, *c* 120°, *d* 150°, *e* 180°

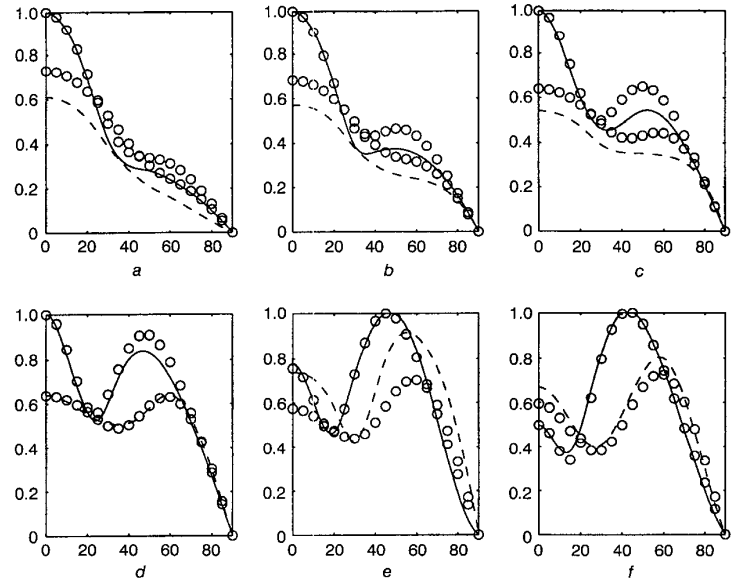

Fig. 8 *Comparison of 60°-flare-angle bowtie field patterns*
The titles refer to the monopole length in electrical degrees
——— Brown and Woodward data for relative electric field strength for plane parallel to bowtie
– – – – Brown and Woodward data for plane normal to bowtie
o moment-model plots
a 195°, *b* 210°, *c* 225°, *d* 240°, *e* 255°, *f* 270°

function of angle in the plane of the bowtie, and the other was the similar measurement in the normal plane. The intersection of the two planes occurs at the axis of the bowtie. Note that Brown and Woodward performed the measurements with respect to angle using a revolving dipole, but then set the relative levels at boresight using measurements taken in the far field of the monopole over the ground plane. (The effect of a finite ground plane on radiation in the equatorial plane is not zero as suggested by [1]. Taking a GTD view, the equatorial plane receives direct and diffracted rays only, and no reflected ray. The loss of the reflected ray would be expected to decrease field strength by half, with diffracted rays varying this somewhat. The argument presented in [1], that horizontal currents in the ground plane can contribute nothing to the vertically polarised far field, is erroneous, since it is precisely such currents which give rise to the vertically polarised reflected field for an infinite ground plane. Consider a TM bundle of rays at glancing incidence: although the reflected ray is approaching the null direction for the hertzian dipoles in the ground plane, the illuminated area of the ground plane, and hence the total source strength, is increasing asymptotically.)

It can be seen that the features of the measured and computed patterns correspond exactly, peaks and nulls occurring at identical angles. The patterns of the 270°- and 240°-length bowties are very close; however, some of the other plots appear to differ by a scaling factor. The worst agreement is seen for the 255° bowtie, where the in-plane measurements are much higher than the calculated fields. If the plots of 50°- and 70°-flare bowties are examined in [1], it can be seen that the peak level of the sidelobe at 255° length lies intermediate between the levels at $A = 240°$ and 270°. The measurements at $\alpha = 60°$ deviate from this smooth behaviour with the peak level at 255° of 0.9, considerably greater than the levels of 0.65 and 0.8 for 240°- and 270°-length bowties. However, the computed field pattern does have a smooth behaviour with the peak level of the in-plane sidelobe of 0.7.

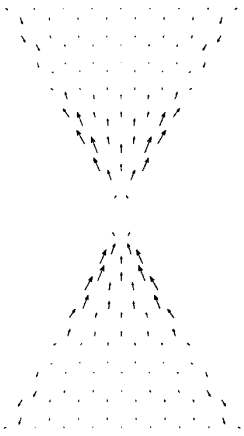

Fig. 9 *Current-density arrow plot for a 60°-flare-angle bowtie of electrical length 270°*
$\omega t = \pi/4$. Note the current concentrations along the edges, and the moving region of zero current, where charges would be most concentrated

One feature of a numerical model is that current-density values can be determined and visualised, without disturbing the distribution. Surface current densities were plotted for the commonly used 60°-flare-angle bowtie, for the electrical monopole length of 270°. Four plots of instantaneous current density are shown for equally spaced intervals in the first half cycle in Figs. 9–11.

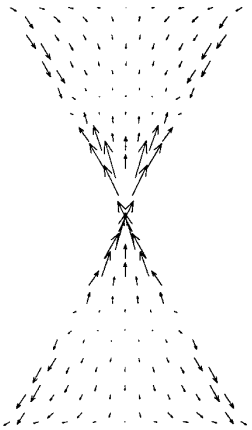

Fig. 10 *Current-density arrow plot for a 60°-flare-angle bowtie of electrical length 270°*
$\omega t = \pi/2$. Note the current concentrations along the edges, and the moving region of zero current, where charges would be most concentrated

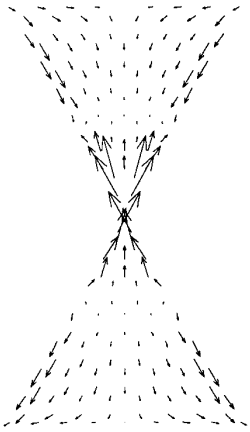

Fig. 11 *Current-density arrow plot for a 60°-flare-angle bowtie of electrical length 270°*
$\omega t = 3\pi/4$. Note the current concentrations along the edges, and the moving region of zero current, where charges would be most concentrated

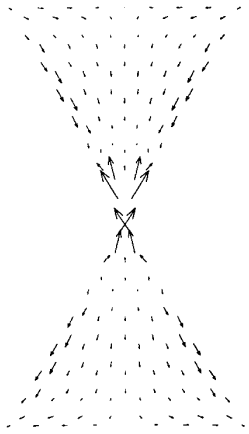

Fig. 12 *Current-density arrow plot for a 60°-flare-angle bowtie of electrical length 270°*
$\omega t = \pi$. Note the current concentrations along the edges, and the moving region of zero current, where charges would be most concentrated

4 Conclusions

A simple, high-speed implementation of the Rao–Wilton–Glisson triangular-basis–function method of

moments has been shown to agree with the well accepted results of Brown and Woodward for the measured impedance and field patterns of bowtie antennas in free space. The use of a delta-function feed model and the Caorsi line-integral method for the self terms can be expected to give equally good results for bowtie antennas in the presence of a half space and shielding, as used in ground-penetrating radar.

5 References

1 BROWN, G.H., and WOODWARD, O.M.: 'Experimentally determined radiation characteristics of conical and triangular antennas', *RCA Rev.*, 1952, pp. 425–452

2 CAORSI, S., MORENO, D., and SIDOTI, F.: 'Theoretical and numerical treatment of surface integrals involving the free space Green's function', *IEEE Trans.*, 1993, **AP–41**, (9), pp. 1296–1301

3 RAO, S.M., WILTON, D.R., and GLISSON, A.W.: 'Electromagnetic scattering by surfaces of arbitrary shape', *IEEE Trans.*, 1982, **AP–30**, (3), pp. 409–418

4 WILTON, D.R., RAO, S.M., GLISSON, A.W., SCHAUBERT, D.H., ALBUNDAK, O.M., and BUTLER, C.M.: 'Potential integrals for uniform and linear source distributions on polygonal and polyhedral domains', *IEEE Trans.*, 1984, **AP–32**, (3), pp. 276–281

5 GRAGLIA, R.D.: 'On the numerical integration of the linear shape function times the 3-d Green's function or its gradient on a plane triangle', *IEEE Trans.*, 1993, **AP–41**, (10), pp. 1448–1455

6 EIBERT, T.F., and HANSEN, V.: 'On the calculation of potential integrals for linear source distributions on triangular domains', *IEEE Trans.*, 1995, **AP–43**, (12), pp. 1499–1502

7 KIPP, R., and CHAN, C.H.: 'Triangular-domain basis functions for full-wave analysis of microstrip discontinuities', *IEEE Trans.*, 1993, **MTT–41**, (6/7), pp. 1187–1194

8 KING, R.W.P.: 'The theory of linear antennas' (Harvard University Press, 1956)